Characterizing biospheric carbon balance using CO_2 observations from the OCO-2 satellite

Scot M. Miller[1], Anna M. Michalak[1], Vineet Yadav[2], and Jovan M. Tadic[3]

[1]Department of Global Ecology, Carnegie Institution for Science, Stanford, CA, USA
[2]Jet Propulsion Laboratory, California Institute of Technology, Pasadena, CA, USA
[3]Lawrence Berkeley National Laboratory, Berkeley, CA, USA

Correspondence to: Scot M. Miller (scot.m.miller@gmail.com)

Abstract.

NASA's Orbiting Carbon Observatory–2 (OCO-2) satellite launched in summer of 2014. Its observations could allow scientists to constrain CO_2 fluxes across regions or continents that were previously difficult to monitor. This study explores an initial step toward that goal; we evaluate the extent to which current OCO-2 observations can detect patterns in biospheric
5   CO_2 fluxes and constrain monthly CO_2 budgets. Our goal is to guide top-down, inverse modeling studies and identify areas for future improvement. We find that uncertainties and biases in the individual OCO-2 observations are comparable to the atmospheric signal from biospheric fluxes, particularly during northern hemisphere winter when biospheric fluxes are small. A series of top-down experiments indicate how these errors affect our ability to constrain monthly biospheric CO_2 budgets. We are able to constrain budgets for between two and four global regions using OCO-2 observations, depending on the month,
10   and we can constrain CO_2 budgets at the regional level (i.e., smaller than seven global ecoregions) in only a handful of cases (16% of all regions and months). The potential of the OCO-2 observations, however, is greater than these results might imply. A set of synthetic data experiments suggests that retrieval errors have a salient effect. Advances in retrieval algorithms and to a lesser extent atmospheric transport modeling will improve the results. In the interim, top-down studies that use current satellite observations are best-equipped to constrain the biospheric carbon balance across only continental or hemispheric regions.

1 Introduction

The OCO-2 satellite launched on July 2nd, 2014 and is NASA's first mission dedicated to observing CO_2 from space. The satellite measures the absorption of reflected sunlight within CO_2 and molecular oxygen (O_2) bands at near infrared wavelengths. These measurements are analyzed with remote sensing retrieval algorithms to yield spatially-resolved estimates of the column-averaged CO_2 dry air mole fraction, XCO_2. The satellite flies in a sun-synchronous orbit an average of 705 km above the Earth's surface, passing each location at approximately 13:30 local time, and it collects roughly 5×10^5 to 1×10^6 observations or soundings per calendar day (e.g., Crisp et al., 2004; Eldering et al., 2012; Crisp et al., 2017).

OCO-2 may provide an ideal opportunity for estimating surface CO_2 fluxes. OCO-2 observes in the near-infrared, and its observations therefore have sensitivity throughout the entire troposphere with highest sensitivity near the surface (e.g., Eldering et al., 2017a). This feature contrasts with several existing satellites that observe in the thermal infrared and have little sensitivity to near-surface CO_2 variations. OCO-2 also has a smaller footprint and improved spatial coverage relative to existing near-infrared observations like those collected by the Greenhouse Gas Observing Satellite (GOSAT). Each OCO-2 observation has a footprint $\sim$2.25km in width, and the satellite can collect eight observations across a single swath (Eldering et al., 2017a). Each GOSAT observation, by contrast, has a footprint $\sim$10km in width, and the satellite collects a single sounding every 250km (Yokota et al., 2009). As a result of these differences, GOSAT provides approximately 1000 high quality observations per day while OCO-2 provides approximately 65000 (e.g., Eldering et al., 2017b).

Prior to the OCO-2 satellite launch, several studies commented on the possibilities of using XCO_2 observations for estimating CO_2 fluxes at the Earth's surface. For example, Chevallier et al. (2007) and Baker et al. (2010) explain that OCO-2 observations could reduce flux uncertainties by $\sim$20–65% at the model grid scale (2.5° by 3.75° and 2° by 5° latitude-longitude, respectively) and at weekly time scales. Both studies, however, caution that biases or spatially and temporally correlated errors would cut this uncertainty reduction in half. Chevallier et al. (2007) further explain that biases of a few tenths of a part per million in XCO_2 could bias estimated subcontinental flux totals by several tenths of a gigaton.

Since launch, a handful of existing studies apply the satellite observations to estimate fluxes for specific problems. Most examine flux anomalies (e.g., El Niño) or anomalously large sources (e.g., power plants). For example, Chatterjee et al. (2017), Patra et al. (2017), Heymann et al. (2017), and Liu et al. (2017) estimate flux anomalies during the most recent El Niño, and Nassar et al. (2017) estimate emissions from several large power plants.

A number of studies use GOSAT observations to estimate surface fluxes, and these studies report numerous successes and challenges that could apply to OCO-2 (e.g., Takagi et al., 2011; Basu et al., 2013; Guerlet et al., 2013; Maksyutov et al., 2013; Parazoo et al., 2013; Saeki et al., 2013; Basu et al., 2014; Deng et al., 2014; Houweling et al., 2015). GOSAT observations provide new insight into fluxes in regions that are poorly sampled by in situ observations. These studies also identify a number of common challenges. For example, observations are too sparse to reliably estimate fluxes in regions with frequent cloud cover (e.g., Parazoo et al., 2013). Furthermore, continental CO_2 budgets estimated using GOSAT observations are not consistent with in situ observations in some regions; these differences may indicate spatially and temporally correlated errors in GOSAT

observations at their current stage of development (e.g., Houweling et al., 2015). These challenges may also be a concern for OCO-2.

This study evaluates the opportunities and challenges of using current OCO-2 observations to estimate biospheric CO_2 fluxes. A primary goal of this work is to guide top down, inverse modeling studies on the information content of currently-available observations. By contrast, satellite capabilities for CO_2 monitoring will likely change quickly over the next ten years – both due to improvements in satellite retrieval algorithms and the launch of new satellites (Sect. 4). This guidance will therefore undoubtedly change and evolve in the future.

We evaluate current OCO-2 observations using several approaches. We first compare model and observation errors against the atmospheric signal from biospheric fluxes. This initial comparison provides context and intuition for the signal-to-noise ratio. Ultimately, atmospheric inversions use more complex patterns in the observations to estimate surface fluxes. We therefore construct a series of top-down simulations using OCO-2 observations to understand what these errors mean for estimating CO_2 fluxes, and we thereby evaluate the number of global regions for which we can independently constrain CO_2 budgets. Lastly, we construct a series of synthetic data simulations to diagnose the real data results. The first synthetic simulations do not include any errors – to evaluate the inherent strengths of the observations. In subsequent synthetic simulations, we include simulated modeling and/or retrieval errors, and evaluate how these errors affect the CO_2 flux constraint.

2 Methods

2.1 OCO-2 data

This study utilizes XCO_2 observations from the OCO-2 satellite beginning with the first reported data (6 Sept. 2014) through the end of 2015. We use the level 2 lite product, version B7.1.01; the lite product only includes good quality retrievals, unlike the full OCO-2 level 2 product. We only include nadir and target mode retrievals in the analysis and exclude glint mode retrievals. Recent work indicates biases in the glint retrievals relative to nadir retrievals (e.g., Wunch et al., 2017). The SI describes model selection results with glint mode retrievals included, and the results are similar to those in the main manuscript without glint mode data.

2.2 Simulated model and retrieval errors

The simulated model and retrieval errors provide an intuitive feel for the observations and are used as inputs in the top-down experiments later on in the study. This section describes these simulated errors – both simulated atmospheric transport and retrieval errors (Fig. 1). The SI describes these errors in greater detail.

We use estimated CO_2 transport errors from Liu et al. (2011) and Miller et al. (2015) (Fig. 1a–b). The authors of those studies run an ensemble of global meteorology simulations. CO_2 is included as a passive tracer in the model, and all simulations use the same CO_2 flux estimate but have different meteorology. The authors estimate CO_2 transport errors by examining the range of CO_2 mixing ratios in the ensemble of simulations. We choose one realization at random and subtract the mean of the ensemble

from this realization to produce a set of residuals. These residuals are used as the estimated transport errors in this study. The estimated errors are therefore a realization of plausible transport errors. As a result, the specific errors used here have the same statistical properties as the other members of the ensemble but have different values in specific locations or at specific times. For example, the transport errors have a negative value across much of the Arctic in Fig. 1a. Other ensemble members might

5   have a slight positive bias in that region but will nevertheless have similar statistical properties as the realization in Fig. 1a.

In addition to these transport errors, we simulate retrieval errors. We use two different approaches to estimate these errors and report results using both approaches. The true retrieval errors are unknown and any effort to estimate these errors will be uncertain; the two approaches used here provide two contrasting, plausible representations of these errors.

We generate the first set of possible retrieval errors using the parameters in the OCO-2 retrieval correction. This approach

10   entails several steps. We first try to reproduce the OCO-2 observations using a regression. The predictor variables in this regression include seven different terrestrial biosphere model (TBM) estimates of net biome production and vegetation indices that have been input into an atmospheric transport model. We also include anthropogenic, ocean, and biomass burning flux estimates in the regression. A subsequent section (Sect. 2.3) describes this regression in greater detail. We save the model-data residuals from this regression. Subsequently, we regress these residuals on the parameters used in the OCO-2 bias correction.

15   These include aerosol optical depth and albedo, among other parameters (e.g., Wunch et al., 2011, see Sect. S1.4). Note that these retrieval parameters are not run through an atmospheric transport model, unlike the TBM fluxes. We estimate the retrieval errors as the portion of the model-observation residuals that are described by these retrieval parameters. The regression considers many different TBMs and vegetation indices, and it should therefore do reasonably well at reproducing patterns in the OCO-2 observations attributable to biospheric fluxes. Any remaining patterns in the data that map on to retrieval parameters

20   are likely due to retrieval errors rather than transport or flux errors.

We use a second approach to create an alternative set of simulated retrieval errors. Specifically, we model XCO_2 using fluxes from four different TBMs (Sect. 2.3) and compute the model-data residuals for each set of simulations. We identify the grid cells in which all four sets of residuals have the same sign (i.e., generated using four different TBMs) and identify all of the model grid cells in which the residuals have variable sign. In the former case, we take the median of all four residuals as the

25   estimated retrieval error and, in the latter case, assign a retrieval error of zero. This approach likely produces a conservative estimate of the retrievals errors (i.e., a possible underestimate); there is likely some amount of retrieval error at locations where we assign a retrieval error of zero.

2.3   Overview of the top-down experiments

We employ a top-down framework to evaluate the detectability of biospheric CO_2 fluxes using current OCO-2 observations.

30   Overall, we divide the globe into different hemispheres and ecoregions and determine whether we can detect flux patterns within each hemisphere or ecoregion and each month. The term 'patterns' here refers to flux patterns that manifest at the resolution of an atmospheric model. We begin the analysis with very large hemispheric regions and then decrease the size of those regions until we are no longer able to detect any flux patterns beyond a mean CO_2 flux. That limit or end point is the smallest scale at which OCO-2 observations currently provide a unique constraint on CO_2 budgets. OCO-2 observations must

be sufficient to detect more than a mean flux across a region and month if future inverse modeling studies are to estimate biospheric CO_2 budgets at scales smaller than that region. Consequently, inverse modeling studies would generally be unable to obtain reliable information about the fluxes across smaller regions. This result bounds the type of information one can expect from the OCO-2 retrievals in their current stage of development. This remainder of this section explains this top-down analysis in greater detail.

We approach this problem using a regression framework. The regression attempts to reproduce OCO-2 observations of XCO_2 using predictor variables. These variables are the XCO_2 estimated by an atmospheric model; each model output estimates the XCO_2 enhancement due to fluxes in a particular region and a particular month, and we generate many model outputs using many different flux models (see Sect. 2.6). The regression has the following form:

$$z \ = \ h(\mathbf{X})\boldsymbol{\beta} + \boldsymbol{b} + \boldsymbol{\epsilon} \tag{1}$$

where $\boldsymbol{z}$ are the OCO-2 observations (dimensions $n \times 1$). The matrix $\mathbf{X}$ ($m \times p$) has p columns, and each column is a different CO_2 flux estimate for specific geographic region and a specific month. Each column of $\mathbf{X}$ has non-zero values for a specific region and month and zeros for all other regions and months. The function $h()$ is an atmospheric transport model (Sect. 2.6), and the model outputs, $h(\mathbf{X})$, have dimensions $n \times p$. The vector $\boldsymbol{b}$ ($n \times 1$) is the model spin-up or estimated XCO_2 at the beginning of the study time period, and $\boldsymbol{\epsilon}$ ($n \times 1$) are the regression residuals. Lastly, $\boldsymbol{\beta}$ ($p \times 1$) are the coefficients estimated as part of the regression.

The regression provides a means to evaluate the detectability of biospheric CO_2 fluxes. At least some of the model outputs ($h(\mathbf{X})$) should describe substantial variability in the OCO-2 observations ($\boldsymbol{z}$). Let's say that modeled XCO_2 using a particular flux model in a particular region and month help reproduce patterns in the OCO-2 observations. This result implies that OCO-2 observations are able to detect or constrain variability in CO_2 fluxes from that region and that month. By contrast, let's say that no model outputs substantially improve the regression fit (i.e., no columns in $h(\mathbf{X})$). This result implies one of three things. First, the OCO-2 observations may not be sensitive to biospheric fluxes from that particular region and month. Second, there may be errors in current OCO-2 retrievals or in the atmospheric model that obscure surface fluxes from that region and month. Finally, all of the flux estimates used in $\mathbf{X}$ may be unskilled and may not match real-world conditions. We offer up a large number of flux models as possible predictor variables in $\mathbf{X}$, and at least some of these products should be expected to correlate with real world CO_2 fluxes. In this case, it is unlikely that there is a shortage of reasonable CO_2 flux models to choose from. Rather, that result more likely reflects the sensitivity of the observations to surface fluxes, the maturity of current OCO-2 retrievals, or the accuracy of the atmospheric model. Hence, this approach provides a means to evaluate when and where current OCO-2 observations can constrain variability in biospheric CO_2 fluxes.

We utilize a model selection framework to determine which model outputs (i.e., columns of $h(\mathbf{X})$) describe substantial variability in current OCO-2 observations. Model selection is a statistical approach common in regression modeling (e.g., Ramsey and Schafer, 2012, ch. 12). It will identify the set of predictor variables with the greatest power to describe the data. It also ensures that the regression does not overfit the data. The inclusion of more predictor variables in a regression will always improve model-data fit; a regression with n independent predictor variables will always be able to describe n data

points perfectly. However, a model with n independent predictor variables would overfit the data. For more on the dangers of overfitting, refer to Zucchini (2000). To this end, one can use model selection to prevent overfitting and only include predictor variables that describe substantial variability in the observations.

We implement model selection based on the Bayesian Information Criterion (BIC) (Schwarz, 1978). We calculate a BIC score for many different combinations of predictor variables, and each combination has a different set of columns ($\mathbf{X}$). The best combination has the lowest BIC score:

$$BIC = L + p\ln(n^*) \tag{2}$$

where L is the log likelihood of a particular combination of predictor variables (i.e., a particular configuration of $\mathbf{X}$). The log likelihood equation rewards combinations that improve model-data fit, and the second term in the equation ($p\ln n^*$) penalizes combinations with a greater number of predictor variables (i.e., columns in $\mathbf{X}$). This penalty also scales with the effective number of independent observations from OCO-2 (n^*, described in the SI), and it ensures that the selected model is not an over-fit.

A number of existing top-down studies of CO_2 use model selection (e.g., Gourdji et al., 2008, 2012; Shiga et al., 2014; Fang et al., 2014; Fang and Michalak, 2015; ASCENDS Ad Hoc Science Definition Team, 2015). Several utilize the approach to determine a set of environmental variables to include in a geostatistical inverse model (e.g., Gourdji et al., 2008, 2012). Other studies use model selection to determine whether existing CO_2 observations can constrain flux patterns from the biosphere (Fang et al., 2014) and from fossil fuel emissions (Shiga et al., 2014; ASCENDS Ad Hoc Science Definition Team, 2015). One study uses model selection to assess the capabilities of a proposed satellite mission (ASCENDS Ad Hoc Science Definition Team, 2015).

Model selection provides a convenient way to evaluate the information content of OCO-2 observations in their current state of development. In theory, one could estimate CO_2 budgets in a Bayesian inverse model. The accuracy or uncertainty in those budgets would be indicative of the information content of the satellite observations. This approach, however, brings several challenges. First, a modeler must choose a prior flux estimate. This choice is often subjective but will impact the final or posterior uncertainty estimate (e.g., Chevallier et al., 2014). Second, a modeler must estimate several individual sources of uncertainty as inputs to the inverse model. These uncertainties often have a complex statistical structure that is difficult to characterize (e.g., Liu et al., 2011), and it is often challenging to account for all plausible sources of uncertainty. Third, inverse modeling with satellite observations can be computationally intensive – both in terms of the number of atmospheric model simulations required and the computational requirements of the statistical inverse model. By contrast, the regression framework used here provides a simpler metric to evaluate the information content of the observations.

2.4 Implementation of the top-down experiments

This section describes how the regression and model selection are implemented in the present study.

The regression begins with an intercept. The intercept is always included in the regression (in $\mathbf{X}$), and model selection can further add flux models to $\mathbf{X}$ to help reproduce the OCO-2 observations ($\mathbf{z}$). This intercept is a constant column of ones in $\mathbf{X}$.

In the particular setup here, we include a different intercept for each region of the globe and each month. In other words, the intercept consists of multiple columns – one column for each region and month of the study period. This intercept is equivalent to a spatially and temporally constant flux in each region and month. Additional atmospheric model outputs $h(\mathbf{X})$ will not be selected unless they explain substantially more variability in the OCO-2 observations than this intercept or constant flux. The intercept plays an important role in the regression; it ensures that the regression will always be unbiased when averaged across the globe. Model selection could produce non-intuitive results if there were no intercept. Furthermore, intercepts are standard in regression modeling, and top-down, CO_2 studies that utilize model selection also include an intercept (e.g., Gourdji et al., 2008, 2012; Fang et al., 2014)

We subsequently run the regression with model selection three times to evaluate three different cases. In the first case, we divide the flux models into two large hemispheric regions, and we select different flux models for each hemispheric region and each month. The second and third experiments divide the fluxes into four continental regions and seven ecoregions, respectively (Fig. 2). The last experiment is more challenging than the first.

Note that we consider the model selection results from 2014 part of an initial model spin-up period and only report the results from 2015.

2.5 Synthetic data simulations

We subsequently utilize synthetic data simulations in this study to analyze the effects of different model or retrieval errors on the detectability of biospheric CO_2 fluxes. In these simulations, we create synthetic XCO_2 observations using an atmospheric transport model (Sect. 2.6) and the SiBCASA flux model. We then run model selection using these synthetic observations in place of real OCO-2 observations ($\mathbf{z}$). These model selection runs have the same setup as the real data simulations, except that the observations are synthetic instead of real. Furthermore, we only analyze the seven ecoregion case in the synthetic data experiments. This case is more demanding of the observations than the two and four region cases; it is more difficult to obtain a robust constraint for seven regions than for two or four larger global regions. The seven ecoregion case is also an important goal from a ecological perspective. For example, one might want to estimate how CO_2 fluxes differ in different tropical forests or in different temperate forests (e.g., on different continents or in different climate zones).

These synthetic simulations help to isolate the effect of different errors on the detectability of biospheric CO_2 fluxes. We first run the regression and model selection with no errors in the atmospheric model or in the retrievals ($\epsilon \approx \mathbf{0}$). We then successively add simulated error to the synthetic observations and evaluate how the model selection results change as the errors increase (Fig. 1). We include three different types of errors: flux errors, transport errors, and retrieval errors. The simulations with all errors included should produce model selection results similar to the real data experiments. Section 2.2 and the SI describe the simulated transport and retrieval errors.

The flux errors further account for plausible inaccuracies in the predictor variables within $\mathbf{X}$. No TBM or vegetation index has a distribution that perfectly matches real-world CO_2 fluxes. These errors affect our ability to detect biospheric fluxes using the OCO-2 observations, and we therefore account for these flux errors in the synthetic data simulations. To this end, we

remove SiBCASA as an option in the $\mathbf{X}$ matrix and choose among the other remaining flux models. This procedure simulates the plausible effects of imperfect flux models or predictor variables.

2.6 Atmospheric model simulations

We employ the Parameterized Chemistry Transport Model (PCTM) to model XCO_2 using a variety of surface flux models
5 (Kawa et al., 2004). A number of existing studies use this model to simulate atmospheric CO_2 mixing ratios (e.g., Law et al., 2008; Gurney et al., 2009; Baker et al., 2010; Schuh et al., 2010; Shiga et al., 2013; ASCENDS Ad Hoc Science Definition Team, 2015; Hammerling et al., 2015). Several of these studies specifically use PCTM to model CO_2 in the context of satellite missions (e.g., Baker et al., 2010; ASCENDS Ad Hoc Science Definition Team, 2015; Hammerling et al., 2015). The PCTM configuration in this study has global coverage, a spatial resolution of $1°$ latitude by $1.25°$ longitude, and 56 vertical levels.
10 We both input the fluxes and estimate atmospheric mixing ratios at a 3-hourly time resolution, and the model transports fluxes through the atmosphere using winds from NASA's Modern-Era Retrospective Analysis for Research and Applications (MERRA) (Rienecker et al., 2011). Section S1.1 includes more detail on the model initial condition and spin-up period.

We subsequently model XCO_2 using several different terrestrial biosphere models (TBMs) and vegetation indices, and these model outputs are incorporated into model selection ($h(\mathbf{X})$). We include four TBMs with contrasting spatial features
15 from MsTMIP, the Multi-scale Synthesis and Terrestrial Model Intercomparison Project (Huntzinger et al., 2013; Fisher et al., 2016a, b). Section S1.2 describes MsTMIP and the TBMs in greater detail. We also include SIF (solar-induced fluorescence) from the Global Ozone Monitoring Experiment-2 (GOME-2, Joiner et al., 2013) as well as EVI (enhanced vegetation index) and NDVI (normalized difference vegetation index) from the Moderate-Resolution Imaging Spectroradiometer (MODIS; e.g., Huete et al., 2002). Note that we directly input these vegetation indices into PCTM as a surface 'flux.' The regression will
20 adjust the magnitude of the transport model outputs to reproduce the OCO-2 observations, so the absolute magnitude of the vegetation indices is not important. Rather, we are interested in whether the patterns in these vegetation indices help reproduce patterns in the OCO-2 observations, potentially in combination with other indices or TBMs.

We also consider non-biospheric fluxes for use in $\mathbf{X}$. We include anthropogenic emissions from EDGAR v4.2 FT2010 (European Commission, Joint Research Centre (JRC)/Netherlands Environmental Assessment Agency (PBL), 2013; Olivier
25 et al., 2014), climatological ocean fluxes from Takahashi et al. (2016), and biomass burning fluxes from the Global Fire Emissions Database (GFED), version 4.1 (van der Werf et al., 2010; Giglio et al., 2013). We are not interested in anthropogenic or marine fluxes per se. Rather, we want to account for these fluxes in the modeling framework and do not want any omissions to affect inferences related to biospheric fluxes. As a result, we do not separate these non-biospheric fluxes by region or month because these sources are not the focus of this study; each of these sources is assigned a single column in $\mathbf{X}$. Furthermore, we
30 do not include these variables by default within $\mathbf{X}$, unlike the constant flux base model. Rather, they are included as candidate variables within the model selection framework.

Note that in the seven ecoregion region case, $\mathbf{X}$ has a minimum of 112 columns and a maximum of 899 columns. 112 columns associated with the intercept and are always included in $\mathbf{X}$ (i.e., 16 months × 7 ecoregions per month). 784 columns associated with biospheric fluxes (7 flux models × 16 months × 7 ecoregions), and three columns associated with fossil fuel,

ocean, and biomass burning fluxes. These columns may or may not be included in $\mathbf{X}$, depending upon the results of model selection.

3 Results & discussion

3.1 The biospheric CO_2 signal versus model and retrieval errors

5   We compare simulated model and retrieval errors against the atmospheric signal from biospheric fluxes (Fig. 3). The comparison provides an intuition of the errors and the CO_2 'signal' given current modeling and observation capabilities. Prior to the OCO-2 satellite launch, several studies modeled the XCO_2 signal from surface fluxes (e.g., Olsen and Randerson, 2004), and the measurement precision required for space-based constraints on CO_2 fluxes (e.g., Rayner and O'Brien, 2001). It is now possible to make this evaluation with real instead of synthetic observations. Also note that the XCO_2 signal and estimated

10   errors will vary depending on the averaging time period. We report monthly averages of the biospheric signal and the errors. Many top-down, inverse modeling studies report monthly flux totals, so all of the analysis presented here is aggregated to one month averages.

     The atmospheric CO_2 signal from biospheric fluxes is marked, even when averaged across a total vertical column (Fig. 3)–a global mean absolute value of 0.5ppm in February and 1.3ppm in July. The 10th and 90th percentiles are 0.04 and 1.4ppm in

15   February and 0.06 and 3.8ppm in July. In July, the largest enhancements are in the northern hemisphere mid and high latitudes while the largest enhancements during winter months are in the tropics and southern hemisphere.

     By contrast, the simulated model and retrieval errors are comparable to this XCO_2 signal from biospheric fluxes. These errors have a mean absolute value of 0.6ppm in both February and July. The 10th and 90th percentiles are 0.08 and 1.35ppm in February and 0.08 to 1.25ppm in July. Using the alternative retrieval estimate, the errors and percentiles are 0.8, 0.02, and

20   2.1ppm in February and 1.4, 0.05, and 3.7ppm in July. Phrased differently, these errors, averaged across all nadir and target data, equate to 115 – 122% of the mean biospheric CO_2 signal in February and 43 – 107% in July, depending upon the retrieval error estimate.

     It is important to note that the distribution of these observations is heterogeneous across the globe (Fig. 3), even though the total number of observations is large (e.g., 268,671 and 343,053 nadir and target observations in February and July, respectively,

25   in the lite data file). For example, the data are concentrated in tropical and temperate regions and are sparse at high latitudes and regions with frequent cloud cover (e.g., the Amazon).

     These errors are not inconsistent with those estimated by existing studies. Wunch et al. (2017) and Liang et al. (2017) compare OCO-2 observations against TCCON observations. Wunch et al. (2017) report an average site bias of 0.22ppm when using land nadir retrievals and a root mean squared error of 1.31ppm. By contrast, Liang et al. (2017) report an error standard

30   deviation of 1.56ppm (both nadir and glint), and find that OCO-2 observations are offset from GOSAT observations by an average of 1.765ppm. In addition, Worden et al. (2017) estimate a precision and accuracy, respectively, of 0.75 and 0.65ppm for land nadir observations. These studies are not necessarily directly comparable because each uses different metrics and

observations. Furthermore, several compare OCO-2 to TCCON, the same observations used to bias correct OCO-2. With that said, the overall numbers reported by different studies are not inconsistent with one another and with Fig. 3.

The relative magnitude of the errors provides an informative measure of the observations, but it does not tell the complete story. A number of other considerations affect scientists' ability to estimate surface fluxes using these observations. First, inverse models leverage more than the point-wise signal to estimate surface fluxes; these models leverage complex spatial and temporal patterns in the data to estimate surface fluxes. Second, the absolute magnitude or variance of the errors is only one consideration. Another important factor is the spatial and temporal correlations or covariances in these errors. These covariances reduce the independent information in the data and can obscure patterns in XCO_2 that are due to surface fluxes. As a result, we construct real and synthetic data experiments to understand what these errors mean for estimating surface fluxes.

3.2 Real data experiments

The model selection experiments using real data indicate the number or size of regions for which we can reliably constrain biospheric CO_2 budgets using current OCO-2 observations. We start the real data simulations with large hemispheric regions and reduce the size of the regions until we are no longer able to detect any CO_2 flux patterns or information beyond a mean monthly flux in each region and each month. We would need to detect more than a mean flux from a given region if we are to reliably constrain fluxes across smaller regions.

The first real data experiment indicates whether the observations are sufficient to detect flux patterns within two large hemispheric regions (Fig. 2). Figure 4a displays the number of months in which at least one model output (i.e., column of $\mathbf{X}$, Eq. 1) is chosen, broken down by region. The results in Fig. 4a are grouped by season for convenience.

Model selection identifies flux patterns in about half of all months. This outcome suggests that OCO-2 and the PCTM model can be used to identify broad, hemispheric flux patterns. One important exception is the extra-tropics (e.g., the temperate, boreal, and arctic region), in both spring and fall. Biospheric uptake in these seasons is less than the summer maximum, in both the northern and southern hemispheres. As a result, flux patterns in these areas are not as heterogeneous and not readily detectable using the satellite observations. This result also indicates that the OCO-2 observations can be used to reliably constrain CO_2 budgets at scales smaller than hemispheric in about half of all cases. With that said, we do not select a single flux pattern in three of four seasons for one hemisphere.

In a second experiment, we try to identify flux patterns within four, smaller regions using OCO-2 observations and model selection (Fig. 4b). At least one flux pattern is selected in 29% of all regions and months, and this result suggests that inverse modeling studies would be able to constrain CO_2 budgets at more detailed spatial scales in about one third of all regions and months. This experiment is more demanding than the first, and it is therefore unsurprising that fewer flux patterns are selected. Flux patterns within these four continental regions are often less heterogeneous than across the two large hemispheric regions in the first experiment.

The third and final experiment includes seven ecoregions, and relatively few flux patterns are selected in this final experiment (16% of all possible regions and months, Fig. 4c). This result suggests a limited ability to detect biospheric flux patterns within each of the seven global ecoregions. Inverse modeling studies would thus be able to uniquely constrain CO_2 budgets across

smaller regions in only a small handful of cases (e.g., 16% of all possible regions and months). These results appear similar to a recent study using current GOSAT retrievals. Houweling et al. (2015) compare an ensemble of inverse modeling flux estimate using GOSAT. Estimates show good agreement across very large regions (e.g., within 20% for global, annual CO_2 budgets) but disagree by over 100% over subcontinental-sized TransCom regions (e.g., Gurney et al., 2002).

5   As part of model selection, we also evaluate the effective number of independent OCO-2 observations (n^*, Sect. S1.3), and we estimate one independent observation per $\sim$1200 OCO-2 lite retrievals. Correlations or covariances in transport and retrieval errors will reduce the value of n^*. The estimate is similar among all of the real data experiments and is approximately 4000 (4060 for the two region case, 3600 for the four region case, and 3540 for the seven region case). By comparison, the total number of OCO-2 observations during the study period (n) is 5.08×10^6. Note that the value of n^* decreases as the number of

10   regions increases. Fewer and fewer model outputs are selected as the number of regions increases. As a result, there are more residual, unexplained flux patterns in the seven region case than in the two region case. As a result, the regression residuals have larger covariances in the seven region case, and the observations become less independent.

These results are broadly consistent with the OCO-2 science team's ongoing flux inter-comparison study (Crowell , 2017). Several research groups are developing inverse models to estimate CO_2 fluxes using OCO-2 observations, and a comparison

15   of these estimates provides insight into the robustness of the flux estimates. To date, these comparisons often show relatively good agreement for total hemispheric terrestrial budgets, but the ensemble of estimates of diverges for smaller regions. Other, newly published inverse modeling studies use OCO-2 observations to estimate regional budgets (e.g., Liu et al., 2017). These studies primarily focus on questions about carbon cycle science, and many employ 4DVAR frameworks that are not necessarily intended to exhaustively sample all plausible sources of uncertainty.

20   ### 3.3   Synthetic data experiments

The goal of the synthetic data simulations is to understand the challenges that influence the real data results. If future efforts can mitigate these challenges, then inverse modeling studies would be able to reliably constrain flux patterns and CO_2 budgets across individual ecoregions or even smaller regions.

We first construct an idealized synthetic data study without any errors (Fig. 5a). This case study indicates that the OCO-2

25   observations are not inherently insensitive to biospheric fluxes at the surface, a result consistent with previous studies (e.g., Olsen and Randerson, 2004). In this idealized case, a flux pattern is selected for every ecoregion in every month using model selection.

Subsequent model selection experiments include at least one error type, and flux patterns are selected in fewer regions and months in all of these cases (Fig. 5b-d). Of the three different error types, retrieval errors have the largest impact on the model

30   selection results (Fig. 5d). Note that the retrieval errors used to generate Fig. 5d are those simulated in Fig. 1c-d. Section S2.2 describes the model selection experiments using an alternative set of retrieval errors (Fig. 1e-f), and these results are similar to those presented in the main manuscript (Fig. 5).

Notably, the addition of any error, large or small, appears to hinder flux pattern detection in marginal ecoregions – ecoregions with small fluxes and/or small spatial and temporal variability (e.g., tundra and deserts). Arguably, this result is unsurprising.

OCO-2 observations are sparse in many cloudy, high latitude regions, and CO_2 fluxes are weak at high latitudes and in deserts. Fluxes from these regions are quickly obscured by even modest errors in the model or observations. Future CO_2 remote sensing efforts would have difficulty detecting biospheric patterns within these areas. Other regions, like forests and grasslands, have larger and/or more heterogeneous fluxes, and these patterns should be easier to detect with satellite observations.

5   One of the experiments specifically accounts for errors in existing flux estimates (Fig. 5b). We find that these errors do have an effect on the results, but that effect is not nearly as large as that due to retrieval errors. We argue that current OCO-2 observations can detect patterns in CO_2 fluxes if at least one model output helps explain substantial variability in those observations. We offer up a number of different model outputs using several different flux models, but there is always a possibility that none of these flux models adequately approximates real world fluxes. The experiment in Fig. 5b evaluates how

10   these flux errors could affect the result. Furthermore, if there are large, unresolved patterns in anthropogenic or marine fluxes, these unresolved patterns could also influence the results for biospheric fluxes. Note that this set of issues also affects Bayesian inverse models and therefore has implications beyond the methodology used in this study. Specifically, the availability and skill of the prior flux estimate affects the robustness and uncertainty of the inverse modeling estimate.

    Subsequent experiments (Fig. 5e-g) include two different error types, and flux patterns are selected in fewer months and

15   regions relative to the previous cases. The experiment with transport and flux errors (but not retrieval errors, Fig. 5e) still show good detectability during the summer months and in temperate and tropical forest and grassland ecoregions. By contrast, the experiments that include retrieval errors (Fig. 5f-g) show limited detectability in all ecoregions and seasons.

    The last experiment (Fig. 5h) includes all error types, and we obtain positive results in fewer regions in fewer months relative to other cases. These results are broadly consistent with the real data experiments; a similar number of regions and seasons are

20   selected in both this experiment and the real data experiment (Fig. 5h). This consistency indicates that the synthetic simulations likely mirror real-world conditions. Note that the estimate for n^* in this final synthetic experiment is about half that of n^* in the real data experiments ($n^* = 1630$). These synthetic experiments may therefore slightly overestimate the error correlations or covariances and underestimate the variance or white noise portion of the errors.

    Overall, the synthetic simulations suggest that retrieval errors play a salient role relative to other error types (e.g., transport

25   errors or flux errors, Fig. 5). Spatial and temporal error covariances and biases may be at least partly to blame. The estimated transport errors are spatially and temporally correlated on synoptic time scales (e.g., Liu et al., 2011; Miller et al., 2015). These scales are generally smaller than the ecoregions and hemispheres examined in this study. As a result, these errors will average down over time and space, and this averaging will mitigate the impact of these errors on the results. This statement, of course, only holds if there are no large-scale biases in the meteorology. The simulated retrieval errors, by comparison, covary across

30   longer spatial and temporal scales. These errors correlate with retrieval parameters like aerosol optical depth or albedo that often change at broader seasonal or regional scales. The greater these error correlations, the less these errors average down across space and time, and the greater impact these errors have on the utility of XCO_2 observations. A reduction in the spatial and temporal coherence of these errors would improve the model selection results.

4 Conclusions

The OCO-2 satellite offers a new, global window into atmospheric CO_2 and CO_2 fluxes at the Earth's surface. This study explores a first step in realizing these capabilities; we evaluate the extent to which current OCO-2 observations can detect patterns in biospheric CO_2 fluxes and constrain monthly CO_2 budgets.

5   We find that OCO-2 observations, in their current state of development, often provide a reliable constraint on CO_2 budgets across continental or hemispheric regions. By contrast, we find that current observations can provide a unique CO_2 estimate across smaller regions in only a handful of cases. As a result, inverse modeling studies are unlikely to constrain regional fluxes at fine spatial and temporal scales given the current maturity of the observations. Regional CO_2 budgets estimated using these observations would be highly uncertain and prone to biases.

10   These results do not reflect any inherent limitation in the sensitivity of the OCO-2 satellite. Rather, a set of synthetic data simulations indicate that these limitations are likely the result of large errors: retrieval errors and to a lesser extent atmospheric transport errors (Fig. 5). Hence, the value or potential of the OCO-2 observations is greater than these results might otherwise imply. For example, the retrieval errors simulated in this study often covary across large regions and across a month or more. Future improvements to retrieval algorithms could reduce both the variance and covariance of these errors, enabling confident

15   CO_2 flux constraints across smaller regions.

Even with these limitations, current OCO-2 observations provide new information on CO_2 fluxes for many regions of the globe. On one hand, in situ data appear to provide a stronger constraint on CO_2 fluxes in some well-instrumented regions of the world, like North America (e.g., Fang et al., 2014). Results using seven global ecoregions show only a limited ability of current OCO-2 observations to differentiate among regions. On the other hand, in situ observations are sparse in many regions

20   of the world, including in most of the tropics, Africa, South America, and Asia (e.g., NOAA Global Monitoring Division, 2017). Current OCO-2 observations bring new monitoring capabilities to these regions that are unlikely to be matched by in situ observations within the near future.

Furthermore, a number of new satellite missions will launch in the next five years. Multiple sets of observations, in tandem, will provide a more detailed, robust constraint on CO_2 fluxes. For example, the GOSAT-2 satellite will monitor atmospheric

25   CO_2 with better accuracy relative to the original GOSAT satellite (Japan Aerospace Exploration Agency, 2017). This improvement in both the quality and overall quantity of CO_2 observations will enable more detailed estimates of CO_2 fluxes. In addition to GOSAT-2, the OCO-3 mission will observe CO_2 from the International Space Station at a different locations and times of day relative to OCO-2 (NASA Jet Propulsion Laboratory, 2017). This feature will provide a stronger constraint on spatial and temporal variations in CO_2 fluxes. However, retrieval errors appear to be a key factor in our results and will likely

30   be a challenge for these future missions. Work on the OCO-2 retrieval algorithm will inform these upcoming missions, so improvements to the OCO-2 retrievals will likely improve the data capabilities of future missions as well. Further improvements to the satellite retrieval and atmospheric transport modeling could enable OCO-2 and future missions to provide detailed CO_2 budgets for much finer regions.

Competing interests. The authors declare that they have no conflict of interest.

Acknowledgements. We thank David Baker, David Crisp, Benjamin Poulter, and Eva Sinha for their help and feedback on the manuscript. The OCO-2 data are produced by the OCO-2 project at the Jet Propulsion Laboratory, California Institute of Technology, and obtained from the OCO-2 data archive maintained at the NASA Goddard Earth Science Data and Information Services Center. OCO-2 data are
5   publicly available online at https://co2.jpl.nasa.gov/#mission=OCO-2. The MODIS EVI and NDVI data products are available online at https://lpdaac.usgs.gov/ courtesy of the NASA Land Processes Distributed Active Archive Center (LP DAAC), USGS/Earth Resources Observation and Science (EROS) Center, Sioux Falls, South Dakota. GOME-2 SIF data are available at https://acd-ext.gsfc.nasa.gov/People/Joiner/my_gifs/GOME_F/GOME-F.htm courtesy of Joanna Joiner. MsTMIP data products are archived at the ORNL DAAC (http://daac.ornl.gov), and 3-hourly flux products are available at dx.doi.org/10.3334/ORNLDAAC/1315. This work is funded by the Carnegie Distinguished Post-
10   doctoral Fellowship and NASA grant #NNX13AC48G. Funding for MsTMIP was provided through NASA ROSES Grant #NNX10AG01A. Data management support for preparing, documenting, and distributing model driver and output data was performed by the Modeling and Synthesis Thematic Data Center at Oak Ridge National Laboratory (ORNL; http://nacp.ornl.gov), with funding thorugh NASA ROSES Grant #NNH10AN681.

References

ASCENDS Ad Hoc Science Definition Team: Active Sensing of CO_2 Emissions over Nights, Days, and Seasons (ASCENDS) Mission: Science Mission Definition Study, NASA, http://cce.nasa.gov/ascends_2015/ASCENDS_FinalDraft_4_27_15.pdf (last access: 30 Aug 2017), 2015.

5 Baker, D. F., Bösch, H., Doney, S. C., O'Brien, D., and Schimel, D. S.: Carbon source/sink information provided by column CO_2 measurements from the Orbiting Carbon Observatory, Atmos. Chem. Phys., 10, 4145–4165, doi:10.5194/acp-10-4145-2010, 2010.

Basu, S., Guerlet, S., Butz, A., Houweling, S., Hasekamp, O., Aben, I., Krummel, P., Steele, P., Langenfelds, R., Torn, M., Biraud, S., Stephens, B., Andrews, A., and Worthy, D.: Global CO_2 fluxes estimated from GOSAT retrievals of total column CO_2, Atmos. Chem. Phys., 13, 8695–8717, doi:10.5194/acp-13-8695-2013, 2013.

10 Basu, S., Krol, M., Butz, A., Clerbaux, C., Sawa, Y., Machida, T., Matsueda, H., Frankenberg, C., Hasekamp, O. P., and Aben, I.: The seasonal variation of the CO_2 flux over Tropical Asia estimated from GOSAT, CONTRAIL, and IASI, Geophys. Res. Lett., 41, 1809–1815, doi:10.1002/2013GL059105, 2014.

Chatterjee, A., Gierach, M. M., Sutton, A. J., Feely, R. A., Crisp, D., Eldering, A., Gunson, M. R., O'Dell, C. W., Stephens, B. B., and Schimel, D. S.: Influence of El Niño on atmospheric CO_2 over the tropical Pacific Ocean: Findings from NASA's OCO-2 mission, 15 Science, 358, doi:10.1126/science.aam5776, 2017.

Chevallier, F., Bron, F.-M., and Rayner, P. J.: Contribution of the Orbiting Carbon Observatory to the estimation of CO_2 sources and sinks: Theoretical study in a variational data assimilation framework, J. Geophys. Res.-Atmos., 112, doi:10.1029/2006JD007375, d09307, 2007.

Chevallier, F., Palmer, P. I., Feng, L., Boesch, H., O'Dell, C. W., and Bousquet, P.: Toward robust and consistent regional CO_2 flux estimates from in situ and spaceborne measurements of atmospheric CO_2, Geophys. Res. Lett., 41, 1065–1070, doi:10.1002/2013GL058772, 20 2013GL058772, 2014.

Crisp, D., Atlas, R., Breon, F.-M., Brown, L., Burrows, J., Ciais, P., Connor, B., Doney, S., Fung, I., Jacob, D., Miller, C., O'Brien, D., Pawson, S., Randerson, J., Rayner, P., Salawitch, R., Sander, S., Sen, B., Stephens, G., Tans, P., Toon, G., Wennberg, P., Wofsy, S., Yung, Y., Kuang, Z., Chudasama, B., Sprague, G., Weiss, B., Pollock, R., Kenyon, D., and Schroll, S.: The Orbiting Carbon Observatory (OCO) mission, Adv. Space Res., 34, 700 – 709, doi:10.1016/j.asr.2003.08.062, 2004.

25 Crisp, D., Pollock, H. R., Rosenberg, R., Chapsky, L., Lee, R. A. M., Oyafuso, F. A., Frankenberg, C., O'Dell, C. W., Bruegge, C. J., Doran, G. B., Eldering, A., Fisher, B. M., Fu, D., Gunson, M. R., Mandrake, L., Osterman, G. B., Schwandner, F. M., Sun, K., Taylor, T. E., Wennberg, P. O., and Wunch, D.: The on-orbit performance of the Orbiting Carbon Observatory-2 (OCO-2) instrument and its radiometrically calibrated products, Atmos. Meas. Tech., 10, 59–81, doi:10.5194/amt-10-59-2017, 2017.

Crowell, S (2017, October). The OCO-2 Level 4 Flux Product. Poster presented at the OCO-2 Science Team Meeting, Boulder, Colorado.

30 Deng, F., Jones, D. B. A., Henze, D. K., Bousserez, N., Bowman, K. W., Fisher, J. B., Nassar, R., O'Dell, C., Wunch, D., Wennberg, P. O., Kort, E. A., Wofsy, S. C., Blumenstock, T., Deutscher, N. M., Griffith, D. W. T., Hase, F., Heikkinen, P., Sherlock, V., Strong, K., Sussmann, R., and Warneke, T.: Inferring regional sources and sinks of atmospheric CO_2 from GOSAT XCO_2 data, Atmos. Chem. Phys., 14, 3703–3727, doi:10.5194/acp-14-3703-2014, 2014.

Eldering, A., Boland, S., Solish, B., Crisp, D., Kahn, P., and Gunson, M.: High precision atmospheric CO_2 measurements from space: The 35 design and implementation of OCO-2, in: 2012 IEEE Aerospace Conference, pp. 1–10, doi:10.1109/AERO.2012.6187176, 2012.

Eldering, A., O'Dell, C. W., Wennberg, P. O., Crisp, D., Gunson, M. R., Viatte, C., Avis, C., Braverman, A., Castano, R., Chang, A., Chapsky, L., Cheng, C., Connor, B., Dang, L., Doran, G., Fisher, B., Frankenberg, C., Fu, D., Granat, R., Hobbs, J., Lee, R. A. M., Mandrake, L.,

McDuffie, J., Miller, C. E., Myers, V., Natraj, V., O'Brien, D., Osterman, G. B., Oyafuso, F., Payne, V. H., Pollock, H. R., Polonsky, I., Roehl, C. M., Rosenberg, R., Schwandner, F., Smyth, M., Tang, V., Taylor, T. E., To, C., Wunch, D., and Yoshimizu, J.: The Orbiting Carbon Observatory-2: first 18 months of science data products, Atmos. Meas. Tech., 10, 549–563, doi:10.5194/amt-10-549-2017, 2017a.

Eldering, A., Wennberg, P. O., Crisp, D., Schimel, D. S., Gunson, M. R., Chatterjee, A., Liu, J., Schwandner, F. M., Sun, Y., O'Dell, C. W., Frankenberg, C., Taylor, T., Fisher, B., Osterman, G. B., Wunch, D., Hakkarainen, J., Tamminen, J., and Weir, B.: The Orbiting Carbon Observatory-2 early science investigations of regional carbon dioxide fluxes, Science, 358, doi:10.1126/science.aam5745, 2017b.

European Commission, Joint Research Centre (JRC)/Netherlands Environmental Assessment Agency (PBL): Emission Database for Global Atmospheric Research (EDGAR), release EDGARv4.2 FT2010, http://edgar.jrc.ec.europa.eu, 2013.

Fang, Y. and Michalak, A. M.: Atmospheric observations inform CO_2 flux responses to enviroclimatic drivers, Global Biogeochem. Cy., 29, 555–566, doi:10.1002/2014GB005034, 2014GB005034, 2015.

Fang, Y., Michalak, A. M., Shiga, Y. P., and Yadav, V.: Using atmospheric observations to evaluate the spatiotemporal variability of CO_2 fluxes simulated by terrestrial biospheric models, Biogeosciences, 11, 6985–6997, doi:10.5194/bg-11-6985-2014, 2014.

Fisher, J. B., Sikka, M., Huntzinger, D. N., Schwalm, C., and Liu, J.: Technical note: 3-hourly temporal downscaling of monthly global terrestrial biosphere model net ecosystem exchange, Biogeosciences, 13, 4271–4277, doi:10.5194/bg-13-4271-2016, 2016.

Schaefer, K., Jacobso, A.R., Arain, M.A., Ciais, P., El-Masri, B., Hayes, D.J., Huang, M., Huang, S., Ito, A., Jain, A.K., Lei, H, Lu, C., Maignan, F., Mao, J., Parazoo, N.C., Peng, C., Peng, S. and Zhu, Q.: CMS: Modeled Net Ecosystem Exchange at 3-hourly Time Steps, 2004-2010. ORNL Distributed Active Archive Center, doi:10.3334/ornldaac/1315, 2016.

Ganesan, A. L., Manning, A. J., Grant, A., Young, D., Oram, D. E., Sturges, W. T., Moncrieff, J. B., and O'Doherty, S.: Quantifying methane and nitrous oxide emissions from the UK and Ireland using a national-scale monitoring network, Atmospheric Chemistry and Physics, 15, 6393–6406, doi:10.5194/acp-15-6393-2015, 2015.

Giglio, L., Randerson, J. T., and van der Werf, G. R.: Analysis of daily, monthly, and annual burned area using the fourth-generation global fire emissions database (GFED4), J. Geophys. Res.-Biogeo., 118, 317–328, doi:10.1002/jgrg.20042, 2013.

Gourdji, S. M., Mueller, K. L., Schaefer, K., and Michalak, A. M.: Global monthly averaged CO_2 fluxes recovered using a geostatistical inverse modeling approach: 2. Results including auxiliary environmental data, J. Geophys. Res. – Atmos., 113, doi:10.1029/2007JD009733, d21115, 2008.

Gourdji, S. M., Mueller, K. L., Yadav, V., Huntzinger, D. N., Andrews, A. E., Trudeau, M., Petron, G., Nehrkorn, T., Eluszkiewicz, J., Henderson, J., Wen, D., Lin, J., Fischer, M., Sweeney, C., and Michalak, A. M.: North American CO_2 exchange: inter-comparison of modeled estimates with results from a fine-scale atmospheric inversion, Biogeosciences, 9, 457–475, doi:10.5194/bg-9-457-2012, 2012.

Guerlet, S., Basu, S., Butz, A., Krol, M., Hahne, P., Houweling, S., Hasekamp, O. P., and Aben, I.: Reduced carbon uptake during the 2010 Northern Hemisphere summer from GOSAT, Geophys. Res. Lett., 40, 2378–2383, doi:10.1002/grl.50402, 2013.

Gurney, K. R., Law, R. M., Denning, A. S., Rayner, P. J., Baker, D., Bousquet, P., Bruhwiler, L., Chen, Y.-H., Ciais, P., Fan, S., et al.: Towards robust regional estimates of CO_2 sources and sinks using atmospheric transport models, Nature, 415, 626–630, doi:10.1038/415626a, 2002.

Gurney, K. R., Mendoza, D. L., Zhou, Y., Fischer, M. L., Miller, C. C., Geethakumar, S., and de la Rue du Can, S.: High resolution fossil fuel combustion CO_2 emission fluxes for the United States, Environ. Sci. Technol., 43, 5535–5541, doi:10.1021/es900806c, pMID: 19708393, 2009.

Hammerling, D. M., Kawa, S. R., Schaefer, K., Doney, S., and Michalak, A. M.: Detectability of CO_2 flux signals by a space-based lidar mission, J. Geophys. Res.-Atmos., 120, 1794–1807, doi:10.1002/2014JD022483, 2014JD022483, 2015.

Heymann, J., Reuter, M., Buchwitz, M., Schneising, O., Bovensmann, H., Burrows, J. P., Massart, S., Kaiser, J. W., and Crisp, D.: CO_2 emission of Indonesian fires in 2015 estimated from satellite-derived atmospheric CO_2 concentrations, Geophys. Res. Lett., 44, 1537–1544, doi:10.1002/2016GL072042, 2016GL072042, 2017.

Houweling, S., Baker, D., Basu, S., Boesch, H., Butz, A., Chevallier, F., Deng, F., Dlugokencky, E. J., Feng, L., Ganshin, A., Hasekamp, O., Jones, D., Maksyutov, S., Marshall, J., Oda, T., O'Dell, C. W., Oshchepkov, S., Palmer, P. I., Peylin, P., Poussi, Z., Reum, F., Takagi, H., Yoshida, Y., and Zhuravlev, R.: An intercomparison of inverse models for estimating sources and sinks of CO_2 using GOSAT measurements, J. Geophys. Res.-Atmos., 120, 5253–5266, doi:10.1002/2014JD022962, 2014JD022962, 2015.

Huete, A., Didan, K., Miura, T., Rodriguez, E., Gao, X., and Ferreira, L.: Overview of the radiometric and biophysical performance of the MODIS vegetation indices, Remote Sens. Environ., 83, 195 – 213, doi:10.1016/S0034-4257(02)00096-2, 2002.

Huntzinger, D. N., Schwalm, C., Michalak, A. M., Schaefer, K., King, A. W., Wei, Y., Jacobson, A., Liu, S., Cook, R. B., Post, W. M., Berthier, G., Hayes, D., Huang, M., Ito, A., Lei, H., Lu, C., Mao, J., Peng, C. H., Peng, S., Poulter, B., Riccuito, D., Shi, X., Tian, H., Wang, W., Zeng, N., Zhao, F., and Zhu, Q.: The North American Carbon Program Multi-Scale Synthesis and Terrestrial Model Intercomparison Project – Part 1: Overview and experimental design, Geosci. Model Dev., 6, 2121–2133, doi:10.5194/gmd-6-2121-2013, 2013.

Japan Aerospace Exploration Agency: GOSAT-2: Greenhouse gas Observing SATellite-2, http://global.jaxa.jp/activity/pr/brochure/files/sat38.pdf (last access: 10 July 2017), 2017.

Joiner, J., Guanter, L., Lindstrot, R., Voigt, M., Vasilkov, A. P., Middleton, E. M., Huemmrich, K. F., Yoshida, Y., and Frankenberg, C.: Global monitoring of terrestrial chlorophyll fluorescence from moderate-spectral-resolution near-infrared satellite measurements: methodology, simulations, and application to GOME-2, Atmos. Meas. Tech., 6, 2803–2823, doi:10.5194/amt-6-2803-2013, 2013.

Kawa, S. R., Erickson, D. J., Pawson, S., and Zhu, Z.: Global CO_2 transport simulations using meteorological data from the NASA data assimilation system, J. Geophys. Res.-Atmos., 109, doi:10.1029/2004JD004554, d18312, 2004.

Law, R. M., Peters, W., Rödenbeck, C., Aulagnier, C., Baker, I., Bergmann, D. J., Bousquet, P., Brandt, J., Bruhwiler, L., Cameron-Smith, P. J., Christensen, J. H., Delage, F., Denning, A. S., Fan, S., Geels, C., Houweling, S., Imasu, R., Karstens, U., Kawa, S. R., Kleist, J., Krol, M. C., Lin, S.-J., Lokupitiya, R., Maki, T., Maksyutov, S., Niwa, Y., Onishi, R., Parazoo, N., Patra, P. K., Pieterse, G., Rivier, L., Satoh, M., Serrar, S., Taguchi, S., Takigawa, M., Vautard, R., Vermeulen, A. T., and Zhu, Z.: TransCom model simulations of hourly atmospheric CO_2: Experimental overview and diurnal cycle results for 2002, Global Biogeochem. Cy., 22, doi:10.1029/2007GB003050, gB3009, 2008.

Liang, A., Gong, W., Han, G., and Xiang, C.: Comparison of Satellite-Observed XCO_2 from GOSAT, OCO-2, and Ground-Based TCCON, Remote Sensing, 9, 2017.

Liu, J., Fung, I., Kalnay, E., and Kang, J.-S.: CO_2 transport uncertainties from the uncertainties in meteorological fields, Geophys. Res. Lett., 38, doi:10.1029/2011GL047213, l12808, 2011.

Liu, J., Bowman, K. W., Lee, M., Henze, D. K., Bousserez, N., Brix, H., Collatz, G. J., Menemenlis, D., Ott, L., Pawson, S., Jones, D., and Nassar, R.: Carbon monitoring system flux estimation and attribution: impact of ACOS-GOSAT XCO_2 sampling on the inference of terrestrial biospheric sources and sinks, Tellus B: Chemical and Physical Meteorology, 66, 22 486, doi:10.3402/tellusb.v66.22486, 2014.

Liu, J., Bowman, K. W., Schimel, D. S., Parazoo, N. C., Jiang, Z., Lee, M., Bloom, A. A., Wunch, D., Frankenberg, C., Sun, Y., O'Dell, C. W., Gurney, K. R., Menemenlis, D., Gierach, M., Crisp, D., and Eldering, A.: Contrasting carbon cycle responses of the tropical continents to the 2015–2016 El Niño, Science, 358, doi:10.1126/science.aam5690, 2017.

Maksyutov, S., Takagi, H., Valsala, V. K., Saito, M., Oda, T., Saeki, T., Belikov, D. A., Saito, R., Ito, A., Yoshida, Y., Morino, I., Uchino, O., Andres, R. J., and Yokota, T.: Regional CO_2 flux estimates for 2009–2010 based on GOSAT and ground-based CO_2 observations, Atmos. Chem. Phys., 13, 9351–9373, doi:10.5194/acp-13-9351-2013, 2013.

Miller, S. M., Hayek, M. N., Andrews, A. E., Fung, I., and Liu, J.: Biases in atmospheric CO_2 estimates from correlated meteorology modeling errors, Atmos. Chem. Phys., 15, 2903–2914, doi:10.5194/acp-15-2903-2015, 2015.

NASA Jet Propulsion Laboratory: Orbiting Carbon Observatory 3, http://www.jpl.nasa.gov/missions/orbiting-carbon-observatory-3-oco-3/ (last access: 30 Aug 2017), 2017.

Nassar, R., Hill, T. G., McLinden, C. A., Wunch, D., Jones, D. B. A., and Crisp, D.: Quantifying CO_2 Emissions From Individual Power Plants From Space, Geophysical Research Letters, 44, 10,045–10,053, doi:10.1002/2017GL074702, 2017GL074702, 2017.

NOAA Global Monitoring Division: Global Greenhouse Gas Reference Network, https://www.esrl.noaa.gov/gmd/ccgg/ggrn.php (last access: 24 Aug 2017), 2017.

Olivier, J., Janssens-Maenhout, G., Munteam, M., and Peters, J.: Trends in global CO_2 emissions; 2014 Report, PBL Netherlands Environmental Assessment Agency; European Commission, Joint Research Centre, Ispra, Italy, http://edgar.jrc.ec.europa.eu/news_docs/jrc-2014-trends-in-global-co2-emissions-2014-report-93171.pdf (last access: 30 Aug 2017), 2014.

Olsen, S. C. and Randerson, J. T.: Differences between surface and column atmospheric CO_2 and implications for carbon cycle research, Journal of Geophysical Research: Atmospheres, 109, doi:10.1029/2003JD003968, d02301, 2004.

Olson, D. M., Dinerstein, E., Wikramanayake, E. D., Burgess, N. D., Powell, G. V. N., Underwood, E. C., D'amico, J. A., Itoua, I., Strand, H. E., Morrison, J. C., Loucks, C. J., Allnutt, T. F., Ricketts, T. H., Kura, Y., Lamoreux, J. F., Wettengel, W. W., Hedao, P., and Kassem, K. R.: Terrestrial ecoregions of the world: A new map of life on Earth, 51, 933–938, doi:10.1641/0006-3568(2001)051[0933:TEOTWA]2.0.CO;2, 2001.

Parazoo, N. C., Bowman, K., Frankenberg, C., Lee, J.-E., Fisher, J. B., Worden, J., Jones, D. B. A., Berry, J., Collatz, G. J., Baker, I. T., Jung, M., Liu, J., Osterman, G., O'Dell, C., Sparks, A., Butz, A., Guerlet, S., Yoshida, Y., Chen, H., and Gerbig, C.: Interpreting seasonal changes in the carbon balance of southern Amazonia using measurements of XCO_2 and chlorophyll fluorescence from GOSAT, Geophys. Res. Lett., 40, 2829–2833, doi:10.1002/grl.50452, 2013.

Patra, P. K., Crisp, D., Kaiser, J. W., Wunch, D., Saeki, T., Ichii, K., Sekiya, T., Wennberg, P. O., Feist, D. G., Pollard, D. F., Griffith, D. W. T., Velazco, V. A., De Maziere, M., Sha, M. K., Roehl, C., Chatterjee, A., and Ishijima, K.: The Orbiting Carbon Observatory (OCO-2) tracks 2–3 peta-gram increase in carbon release to the atmosphere during the 2014–2016 El Niño, Scientific Reports, 7, 13 567, doi:10.1038/s41598-017-13459-0, 2017.

Ramsey, F. and Schafer, D.: The Statistical Sleuth: A Course in Methods of Data Analysis, Cengage Learning, Boston, MA, 2012.

Rayner, P. J. and O'Brien, D. M.: The utility of remotely sensed CO_2 concentration data in surface source inversions, Geophysical Research Letters, 28, 175–178, http://dx.doi.org/10.1029/2000GL011912, 2001.

Rienecker, M. M., Suarez, M. J., Gelaro, R., Todling, R., Bacmeister, J., Liu, E., Bosilovich, M. G., Schubert, S. D., Takacs, L., Kim, G.-K., Bloom, S., Chen, J., Collins, D., Conaty, A., da Silva, A., Gu, W., Joiner, J., Koster, R. D., Lucchesi, R., Molod, A., Owens, T., Pawson, S., Pegion, P., Redder, C. R., Reichle, R., Robertson, F. R., Ruddick, A. G., Sienkiewicz, M., and Woollen, J.: MERRA: NASA's Modern-Era Retrospective Analysis for Research and Applications, J. Climate, 24, 3624–3648, doi:10.1175/JCLI-D-11-00015.1, 2011.

Rigby, M., Manning, A. J., and Prinn, R. G.: Inversion of long-lived trace gas emissions using combined Eulerian and Lagrangian chemical transport models, Atmospheric Chemistry and Physics, 11, 9887–9898, doi:10.5194/acp-11-9887-2011, 2011.

Saeki, T., Maksyutov, S., Saito, M., Valsala, V., Oda, T., Andres, R. J., Belikov, D., Tans, P., Dlugokencky, E., Yoshida, Y., Morino, I., Uchino, O., and Yokota, T.: Inverse modeling of CO_2 fluxes using GOSAT data and multi-year ground-based observations, SOLA, 9, 45–50, doi:10.2151/sola.2013-011, 2013.

Schuh, A. E., Denning, A. S., Corbin, K. D., Baker, I. T., Uliasz, M., Parazoo, N., Andrews, A. E., and Worthy, D. E. J.: A regional high-resolution carbon flux inversion of North America for 2004, Biogeosciences, 7, 1625–1644, doi:10.5194/bg-7-1625-2010, 2010.

Schwarz, G.: Estimating the dimension of a model, Ann. Stat., 6, 461–464, http://www.jstor.org/stable/2958889, 1978.

Shiga, Y. P., Michalak, A. M., Randolph Kawa, S., and Engelen, R. J.: In-situ CO_2 monitoring network evaluation and design: A criterion based on atmospheric CO_2 variability, J. Geophys. Res.-Atmos., 118, 2007–2018, doi:10.1002/jgrd.50168, 2013.

Shiga, Y. P., Michalak, A. M., Gourdji, S. M., Mueller, K. L., and Yadav, V.: Detecting fossil fuel emissions patterns from subconti-nental regions using North American in situ CO_2 measurements, Geophys. Res. Lett., 41, 4381–4388, doi:10.1002/2014GL059684, 2014GL059684, 2014.

Takagi, H., Saeki, T., Oda, T., Saito, M., Valsala, V., Belikov, D., Saito, R., Yoshida, Y., Morino, I., Uchino, O., Andres, R. J., Yokota, T., and Maksyutov, S.: On the benefit of GOSAT observations to the estimation of regional CO_2 fluxes, SOLA, 7, 161–164, doi:10.2151/sola.2011-041, 2011.

Takahashi, T., Sutherland, S., and Kozyr, A.: Global Ocean Surface Water Partial Pressure of CO_2 Database: Measurements Performed During 1957-2015 (Version 2015)., ORNL/CDIAC-160, NDP-088(V2015), Oak Ridge National Laboratory, U.S. Department of Energy, Oak Ridge, Tennesee, doi:10.3334/CDIAC/OTG.NDP088(V2015), 2016.

van der Werf, G. R., Randerson, J. T., Giglio, L., Collatz, G. J., Mu, M., Kasibhatla, P. S., Morton, D. C., DeFries, R. S., Jin, Y., and van Leeuwen, T. T.: Global fire emissions and the contribution of deforestation, savanna, forest, agricultural, and peat fires (1997–2009), Atmos. Chem. Phys., 10, 11 707–11 735, doi:10.5194/acp-10-11707-2010, 2010.

Worden, J. R., Doran, G., Kulawik, S., Eldering, A., Crisp, D., Frankenberg, C., O'Dell, C., and Bowman, K.: Evaluation and attribution of OCO-2 XCO2 uncertainties, Atmospheric Measurement Techniques, 10, 2759–2771, doi:10.5194/amt-10-2759-2017, 2017.

Wunch, D., Wennberg, P. O., Toon, G. C., Connor, B. J., Fisher, B., Osterman, G. B., Frankenberg, C., Mandrake, L., O'Dell, C., Ahonen, P., Biraud, S. C., Castano, R., Cressie, N., Crisp, D., Deutscher, N. M., Eldering, A., Fisher, M. L., Griffith, D. W. T., Gunson, M., Heikkinen, P., Keppel-Aleks, G., Kyrö, E., Lindenmaier, R., Macatangay, R., Mendonca, J., Messerschmidt, J., Miller, C. E., Morino, I., Notholt, J., Oyafuso, F. A., Rettinger, M., Robinson, J., Roehl, C. M., Salawitch, R. J., Sherlock, V., Strong, K., Sussmann, R., Tanaka, T., Thompson, D. R., Uchino, O., Warneke, T., and Wofsy, S. C.: A method for evaluating bias in global measurements of CO_2 total columns from space, Atmos. Chem. Phys., 11, 12 317–12 337, doi:10.5194/acp-11-12317-2011, 2011.

Wunch, D., Wennberg, P. O., Osterman, G., Fisher, B., Naylor, B., Roehl, C. M., O'Dell, C., Mandrake, L., Viatte, C., Kiel, M., Griffith, D. W. T., Deutscher, N. M., Velazco, V. A., Notholt, J., Warneke, T., Petri, C., De Maziere, M., Sha, M. K., Sussmann, R., Rettinger, M., Pollard, D., Robinson, J., Morino, I., Uchino, O., Hase, F., Blumenstock, T., Feist, D. G., Arnold, S. G., Strong, K., Mendonca, J., Kivi, R., Heikkinen, P., Iraci, L., Podolske, J., Hillyard, P. W., Kawakami, S., Dubey, M. K., Parker, H. A., Sepulveda, E., García, O. E., Te, Y., Jeseck, P., Gunson, M. R., Crisp, D., and Eldering, A.: Comparisons of the Orbiting Carbon Observatory-2 (OCO-2) X_{CO_2} measurements with TCCON, Atmos. Meas. Tech., 10, 2209–2238, doi:10.5194/amt-10-2209-2017, 2017.

Yokota, T., Yoshida, Y., Eguchi, N., Ota, Y., Tanaka, T., Watanabe, H., and Maksyutov, S.: Global Concentrations of CO_2 and CH_4 Retrieved from GOSAT: First Preliminary Results, SOLA, 5, 160–163, doi:10.2151/sola.2009-041, 2009.

Zucchini, W.: An Introduction to Model Selection, J. Math. Psychol., 44, 41 – 61, doi:10.1006/jmps.1999.1276, 2000.
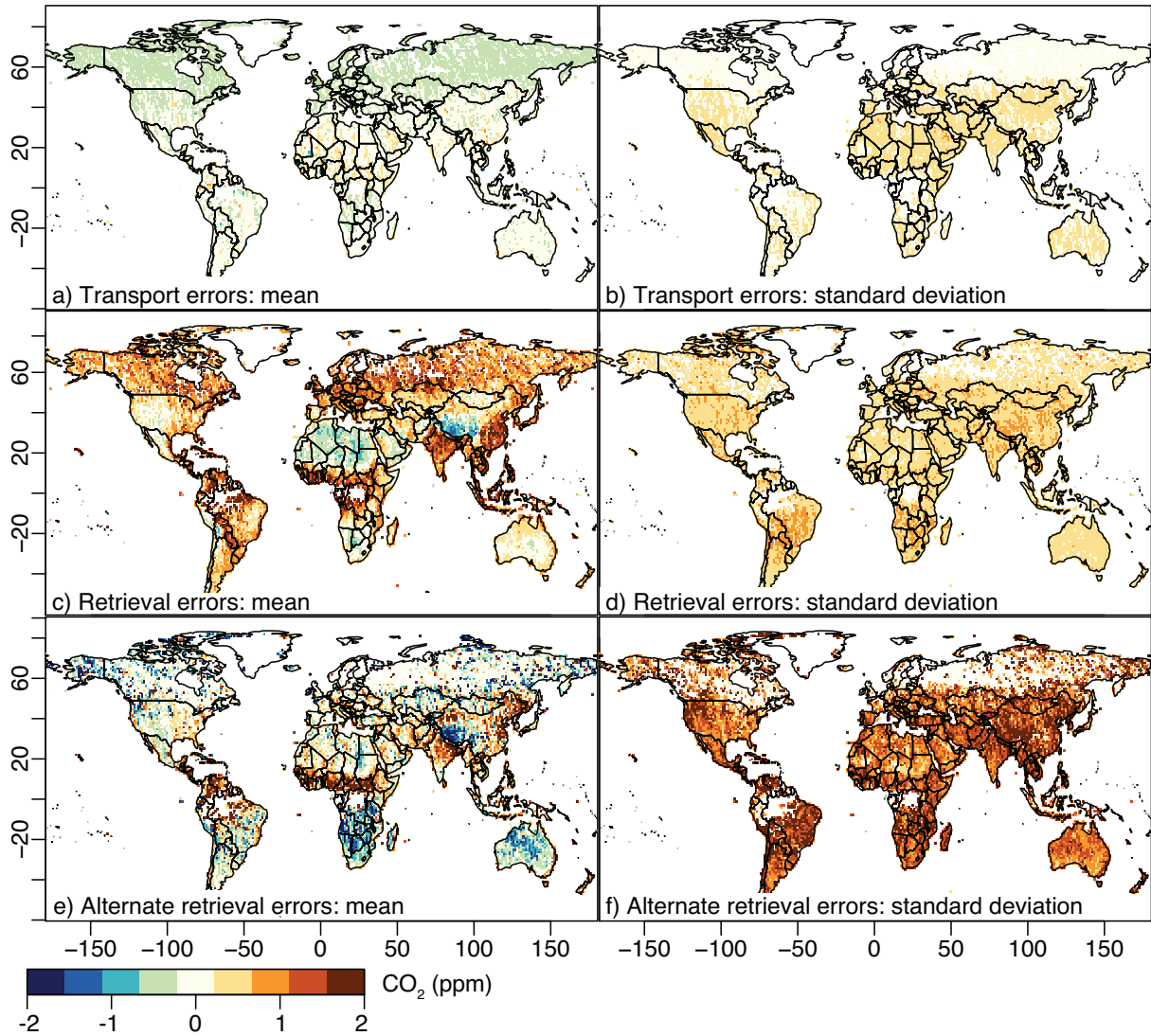
Figure 1. This figure displays the simulated synthetic data errors (i.e., simulated ϵ): the simulated atmospheric transport errors (a-b), the simulated observation/retrieval errors (c-d), and a second, alternative set of observation/retrieval errors (e-f). The left-hand panels display the mean of the errors within each PCTM grid box across the entire 2014–2015 study period, an indication of the correlation or covariance among the errors. By contrast, the right-hand panels display the standard deviation of the errors or residuals within each PCTM grid box.
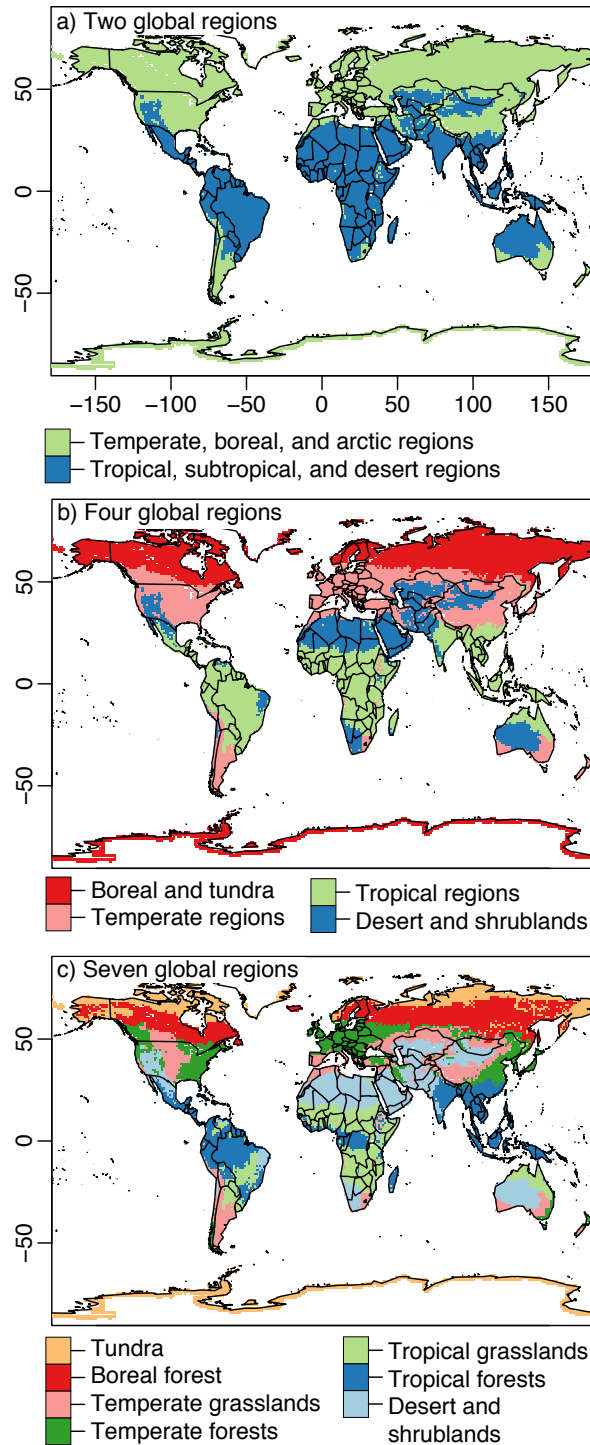
Figure 2. The two hemispheric regions (a), four continental regions (b), and seven ecoregions (c) used in this study. The ecoregions are based on a world biome map by Olson et al. (2001). The two and four region maps are amalgamated versions of the ecoregions.
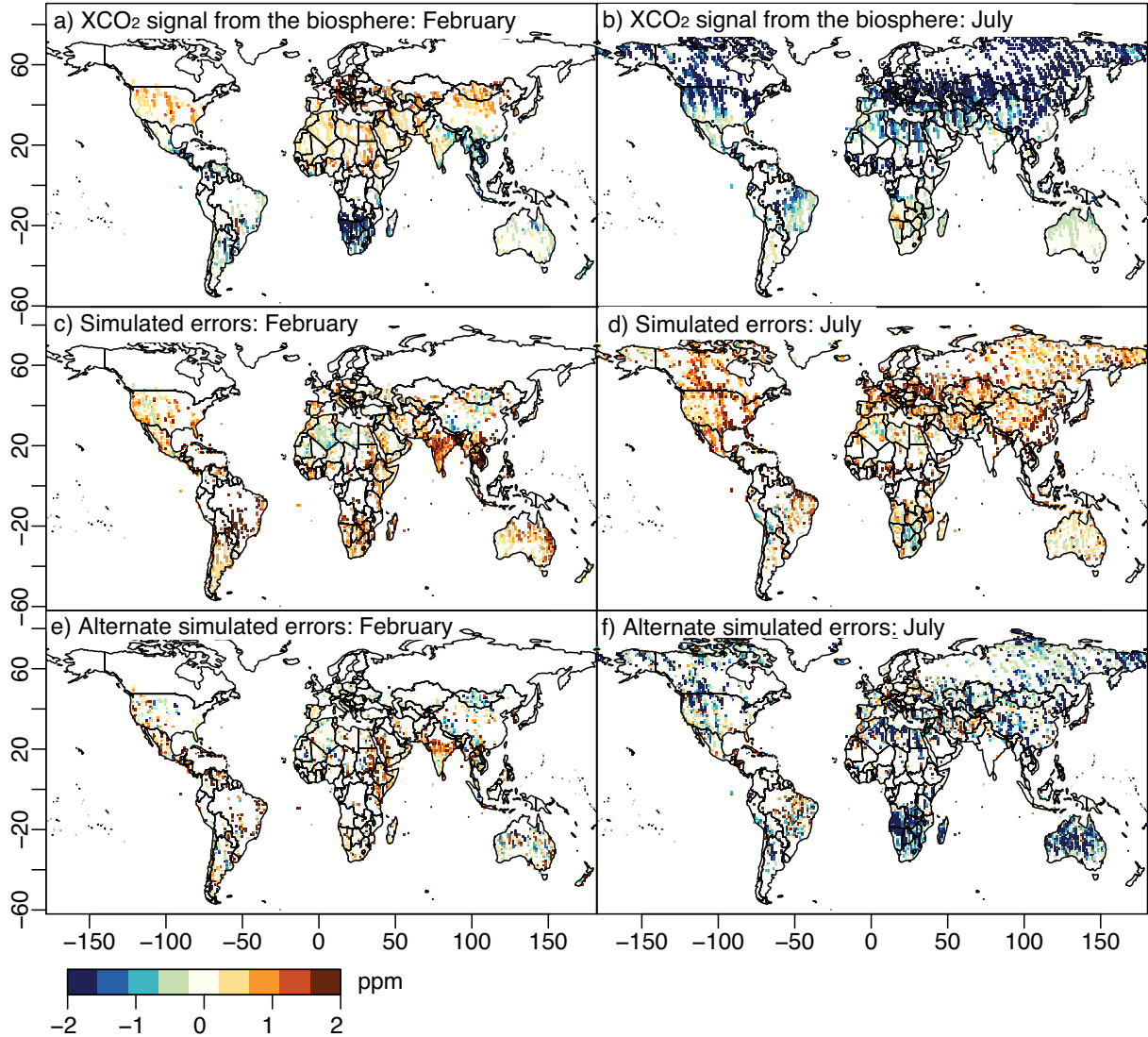
Figure 3. This figure compares the total column CO_2 or XCO_2 signal from biospheric fluxes against simulated model and observation errors. Panels a and b display the monthlong mean XCO_2 signal from biospheric CO_2 fluxes for February and July, respectively. We estimate this signal using the SiBCASA flux model and PCTM. Also note that the XCO_2 signal for February and July includes CO_2 fluxes from the months of February and July, respectively, and no fluxes from previous or subsequent months. Panels c and d represent the sum of both simulated observation and atmospheric transport errors (monthlong mean, Sect. 2.2). Panels e and f show the sum of these errors using an alternate estimate for the retrieval errors.
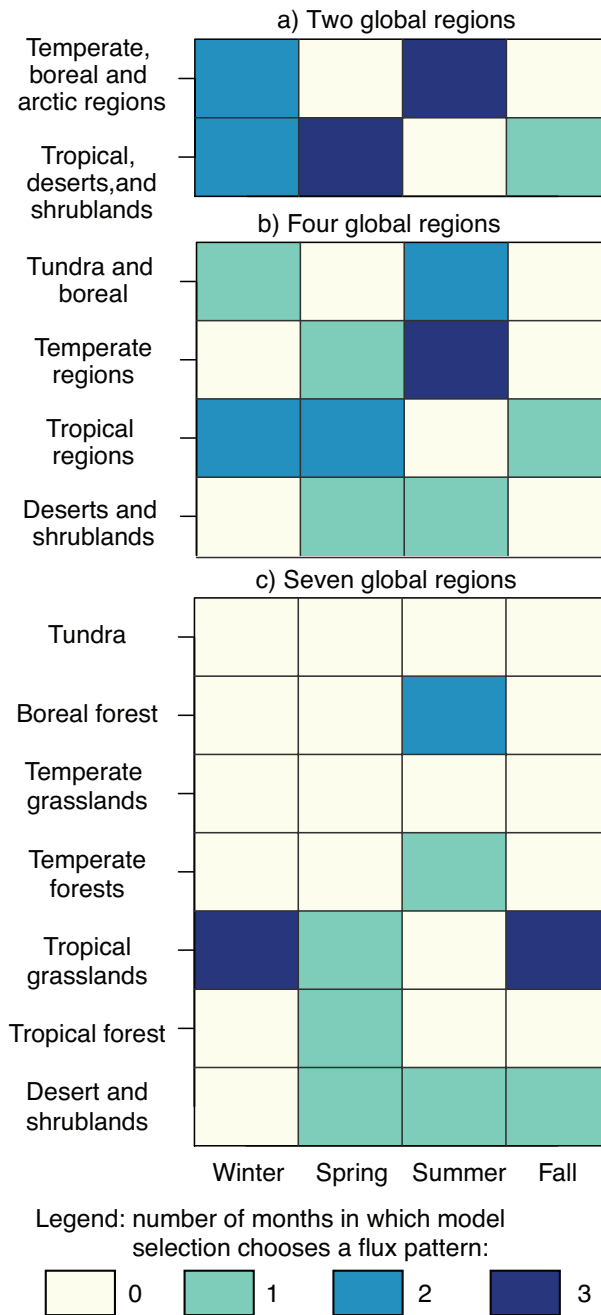
Figure 4. The results of the model selection experiments using real data. The different colors indicate the number of months in which at least one flux pattern is selected for a given region, and dark colors suggest excellent detectability while light colors suggest limited detection abilities. Flux patterns are selected for a greater fraction of regions/months in the two region case (a) than in the four or seven region cases (b and c).
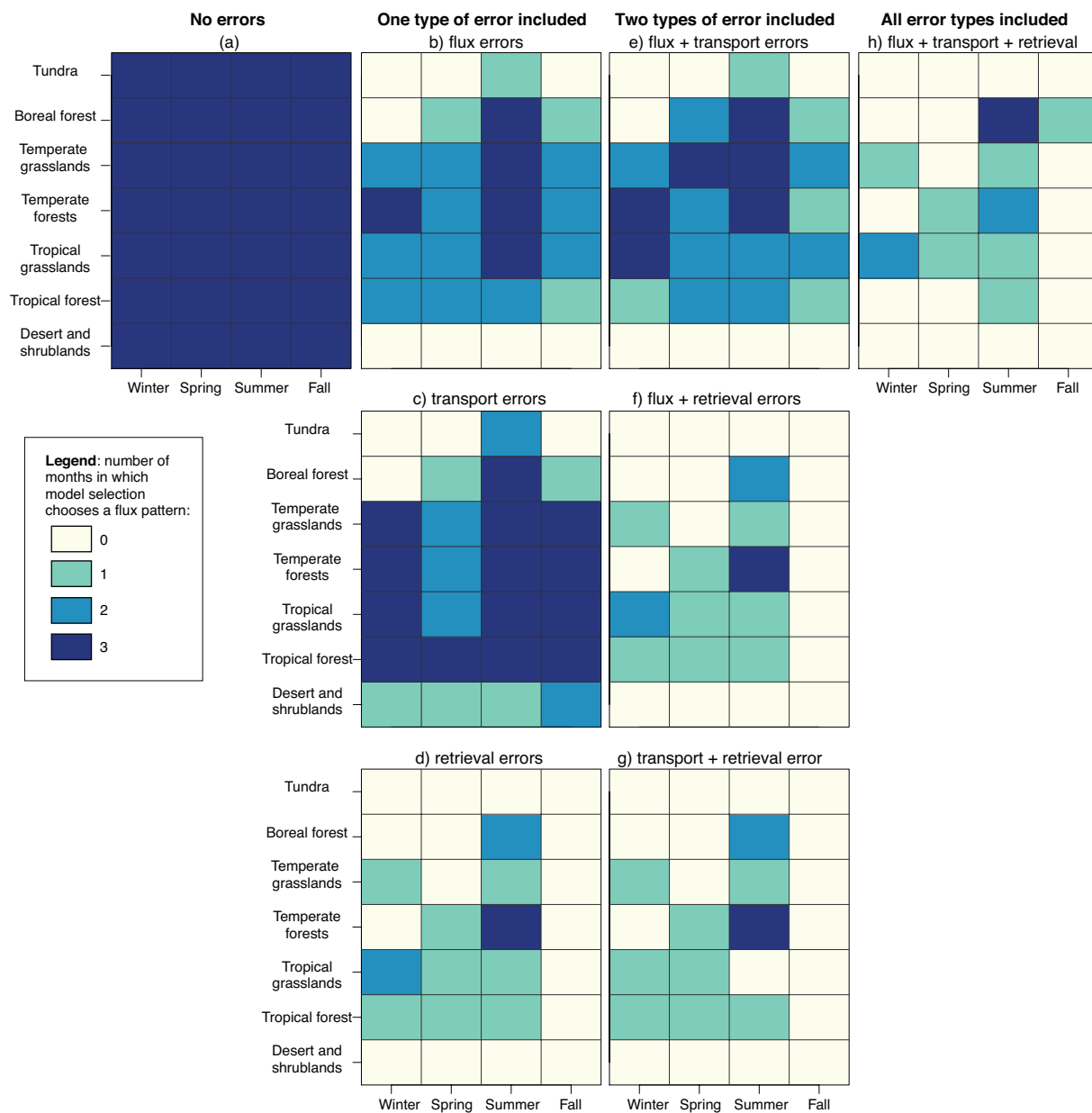
Figure 5. Model selection results for the synthetic data experiments. The first column (a) shows an experiment with no errors in the synthetic observations. The results of that experiment are ideal, and at least one flux pattern is selected in every month and every region using model selection. Subsequent panels (b-h) show the results with one, two, and three types of errors included. Fewer regions and seasons are selected in these experiments. The plot signals that retrieval errors likely play a key role.